HEAT TRANSFER LOSSES IN RECIPROCATING COMPRESSORS WITH VALVE ACTUATION FOR ENERGY STORAGE APPLICATIONS

C. Willich*, A. J. White

Department of Engineering, University of Cambridge, UK
c.willich@eng.cam.ac.uk

Keywords: exergetic loss, irreversible heat transfer, gas spring, reciprocating compressor

Abstract

Understanding the exergy losses stemming from heat transfer in compressors and expanders is important for many energy storage applications such as compressed air and pumped thermal storage. In order to obtain a better understanding of these losses, CFD simulations were performed for simple gas springs, for a gas spring with an internal grid to mimic valve flow, and for a reciprocating compressor with functioning inlet and outlet valves. The wall heat exchanges for these three cases were examined and compared. The model adopted has previously been validated for a simple gas spring using experimental data from literature. For the gas spring with an internal grid it was found that increased mixing leads to higher heat-transfer-induced hysteresis losses and (at high piston speeds) to a significant pressure loss. These two types of loss can be distinguished by undertaking adiabatic-wall calculations. For a compressor (i.e., with valve flows) heat transfer over the cycle depends very much on valve timing. For example, at 1500 rpm, when the delivery valve is opened at 7 bar the heat transfer coefficient for the initial stages of compression is similar to that for a simple gas spring, whereas for the same speed at 6 bar it is more than doubled.

1 Introduction

To achieve a reliable and sustainable energy supply the percentage of electrical energy from renewable sources will increase strongly within the next years. Since many of these sources (particularly wind and solar energy) do not provide continuous supplies and since the demand for power varies over the day and over the year, electricity storage is seen as increasingly important for a sustainable energy system.

Aside from their common use in internal combustion engines, reciprocating compressors and expanders have a wide range of applications in energy storage devices and energy systems in general. They are potentially important, for instance, for compressed air energy storage (CAES), and pumped thermal energy storage (PTES), and they may also be used in combined heat and power (CHP) [1], heat pumps [2] and Stirling engines for solar applications [3]. In the case of PTES (which is the focus of the current study), previous work has shown that compression and expansion losses have a major impact on the overall (round-trip) efficiency, essentially because the complete charge-discharge process involves two compressions and two expansions [4].

The main sources of loss in reciprocating compressors and expanders are likely to be valve pressure losses and heat transfer irreversibility. Whereas pressure losses may be reduced by maximizing the valve open area and optimising the valve timing, trends for heat-transfer-related loss are less obvious. To better understand heat transfer effects, various researchers have examined the processes occurring in a gas spring [5, 6, 7] – i.e., a reciprocating piston within a cylinder, but without any valves. This enables examination of heat transfer loss independently of losses incurred by the valve flows, but in a real compressor the behaviour will be considerably different since mass is exchanged during every cycle, and the incoming flow generates turbulence, thereby affecting rates of heat transfer. The incoming and outgoing gas also transports energy to and from the cylinder.

This paper examines the heat transfer losses in a reciprocating device by means of CFD simulations. In the first step a gas spring without any valves was studied. Simulations were carried out for a wide range of piston speeds and for two geometries with two different gases (air and helium) and these were used for the validation of the model. Helium was used since experimental data for the validation of the model is available from the literature [7, 5] and air because an experimental setup using air is currently under development, as described by Mathie et al [6]. In a second step, mixing inside the cylinder was increased by inserting a grid. This was intended to mimic the turbulence generated by valve flows. These simulations are described in greater detail elsewhere [8] but are summarised here for completeness. In the last step the CFD model was adapted to include valve flows so that differences between heat transfer for a gas spring and a real compressor with mass through-flow could be examined.

The simulations with valves require substantial computing time to obtain converged solutions and only three operating

*Current affiliation: Catalonia Institute for Energy Research (IREC), Barcelona, Spain

conditions have so far been computed. Although this is not sufficient to give a full picture of exergetic losses (this being the ultimate aim), the results obtained highlight some important qualitative differences between gas springs and real compressors (or expanders) and provide valuable information for the design of on-going simulations.

2 Computational method and model validation

Simulations were performed using the 'coldEngineFoam' solver of OpenFOAM [9], version 2.3.0, which is a solver for 'cold' (non-combustion) flow in internal combustion engines. It includes mesh motion for the moving piston and uses the PIMPLE transient solver for incompressible flow. PIMPLE is a combination of the PISO (Pressure implicit with splitting of operator) and SIMPLE (Semi-Implicit Method for Pressure Linked Equations) algorithms. PISO solves velocity-pressure coupling for each time step by predicting the velocity field from an initial guess of pressure and then correcting pressure and velocity to satisfy mass conservation. The correction step is then repeated. In the PIMPLE algorithm an outer correction loop can be used which iterates over the same time step using the last value as input for the next iteration, while under-relaxing variables between these outer iterations.

The model used in this study assumes perfect gas relations with constant heat capacity c_p, constant dynamic viscosity μ and constant Prandtl number. Reynolds-averaged simulations (RAS) based on a k-epsilon model are used for modelling turbulence. This is suitable for flows with small pressure gradients and no separation [10] and is less computationally intense than other models [11]. Note that although the solver is appropriate only for *incompressible* flow, this does not restrict it to constant density, which of course varies with the position of the piston. Mach numbers in the modelled domain are however typically less than 0.06 (when the Mach number is lower than 0.3 compressibility effects are negligible [8]), so local changes in pressure spread through the whole volume rapidly such that a new pressure with only small gradients is reached in each time step [12]. An incompressible solver like coldEngineFoam is therefore be most suitable, although other reciprocating compression studies have been undertaken with compressible solvers [13].

The gas spring simulations were first checked for reliability: the CFD results were compared to theory for adiabatic and isothermal compression, and for pressure differences and axial velocity variations between the piston and cylinder head. Agreement was found to be very good, as detailed in Ref. [8]. Fig. 1 for instance shows pressure-volume (*p-V*) curves for different piston speeds. At high speed (1500 rpm) the forward and backward curves are very close together, indicating near-reversible processes. (The lost work is given by the area enclosed between the curves and is very small.) Compression and expansion are nearly adiabatic because there is insufficient time for heat transfer and consequently the curves lie close to the isentropic *p-V* curve, as shown in the figure (black symbols). For very low piston speed (0.01 rpm) the backward and forward curves are again nearly coincident, but this time lie close to the isothermal process (grey symbols), reflecting the fact that the gas is almost in thermal equilibrium with the cylinder walls. At intermediate speeds (e.g., 2 rpm) heat transfer occurs across significant temperature differences and the resulting irreversibility manifests itself as lost work and hence a difference between the forward and backward *p-V* curves.

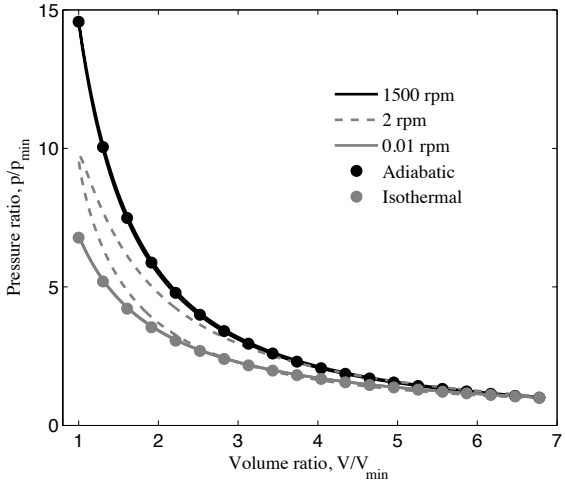

Figure 1: Computed *p-V* curves for different piston speeds at compression ratio $r_v = 6.8$. The isothermal and adiabatic (isentropic) relations ($pV = \text{const.}$ and $pV^{\gamma} = \text{const.}$) are also shown.

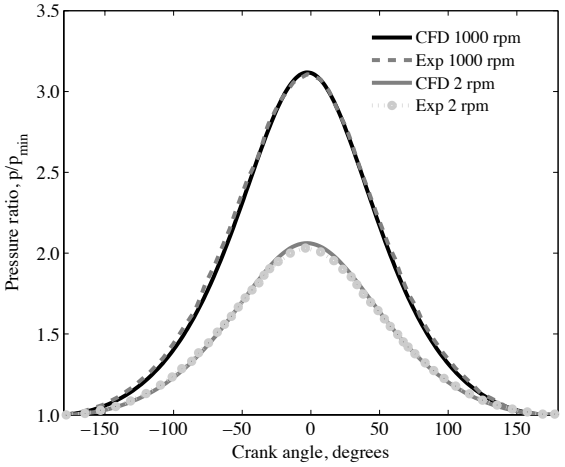

Figure 2: Pressure *vs.* crank angle (CA) for 1000 rpm and 2 rpm. Experimental values and geometry are taken from [5]. The working fluid is helium.

The CFD results were further compared to experimental data available in the literature. Fig. 2 for instance shows the pressure against crank angle for two different piston speeds (note 0° corresponds to top dead centre, TDC). CFD results are compared with experimental data from [5] and generally

show good agreement. No tuning was applied to achieve the agreement shown, here or elsewhere.

2.1 Wall heat fluxes

Wall heat fluxes are computed directly from

$$q_w = -k\frac{\partial T}{\partial n} \qquad (1)$$

where k is the gas thermal conductivity and n is the distance normal to the wall. Negative values correspond to heat loss from the gas. For gas springs (for which the gas constitutes a closed system) average heat fluxes may also be computed from the First Law and accord well with those obtained from eq. (1), as detailed in Ref. [8].

3 Geometry and simulation parameters

3.1 Gas spring geometry

For simple gas springs, two geometries were studied. Geometry 1 (table 1) has a low volume compression ratio of $r_v = 2$ and corresponds to the experiments by Kornhauser and Smith [14]. The other geometry corresponds to that under development by Mathie et al [6], for which $r_v = 6.8$. To minimise computing times, only a slice (5°) from the axisymmetric cylinder was simulated. (One simulation for a whole cylinder at 1500 rpm was also conducted but showed no discernable differences in pressures or temperatures.)

Geometry	Radius [mm]	Stroke [mm]	Clearance [mm]	Con rod length [mm]	Volume ratio, r_v
1 [5]	25.4	76.2	76.2	183	2.00
2 [6]	52.5	78.0	13.5	150	6.85

Table 1: Geometries of simulated cylinders

The simulations including a turbulence grid were done using geometry 1 with helium as working fluid. A quarter cylinder was simulated with a baffle containing 12 holes each of size 5×2.5 mm. This results in an open area of 29.6%. The grid was inserted 65.4 mm below the cylinder head and 10.8 mm away from the piston at TDC, as shown in Fig. 3. Supporting data for the gas spring simulations can be found at http://dx.doi.org/10. 17863/CAM.4828.

3.2 Compressor geometry

All valve simulations were done with geometry 2. The design of the valves was based loosely on the valve system described by Howes [15], intended for a PTES system. The valve setup differs from conventional piston compressors because the outlet valve is in the piston face and the inlet is in the cylinder head, giving a uni-flow configuration. The valves consist of plates with an array of rectangular holes. This design aims at maximising the open area and avoiding any large-scale swirl when gas is entering the cylinder.

Figure 3: Cylinder without and with turbulence grid with streamlines at TDC for geometry 1 [8].

When closing the valves a second plate slides across the open areas thus sealing them. In the simulations, this second plate is assumed to slide completely out of the way when opening the valves, so that there is no obstacle blocking the flow through the holes. Valves were thus modelled by changing the boundary conditions to an inlet or outlet when open and back to solid wall when closed. This is of course a simplification as in reality sliding of the valves as well as the fluid movement outside the cylinder impacts on the performance. A quarter cylinder was simulated in which the valves comprised 12 open areas of 5×10 mm (roughly 28% of the piston face), as shown in Fig. 4.

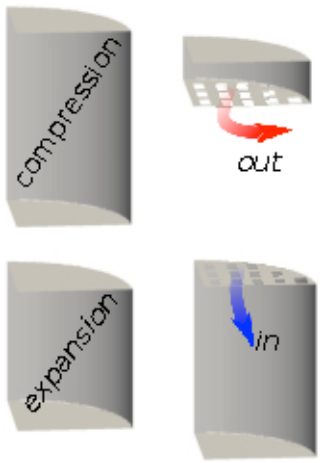

Figure 4: Opening and closing of valves for geometry 2

3.3 Operating and boundary conditions

For precise modelling of a real device (compressor, expander or gas spring), wall boundary conditions must be determined by solving the conjugate heat transfer problem, accounting for heat exchange between the cylinder and surroundings. For simplicity, however, the present calculations were undertaken with isothermal wall conditions with uniform temperature.

Nonetheless, there is a qualitative difference between the gas spring and valved device, thus requiring a different treatment, as described below.

3.3.1 Gas springs

All gas spring simulations were with a fixed wall temperature of 300 K and were started from bottom dead centre (BDC) with the gas also initially at 300 K and 1 bar. These initial conditions determine the mass of gas inside the cylinder. The temperature of the gas (averaged over the volume and over the cycle) falls for the first few cycles such that the minimum and maximum temperatures (near BDC and TDC respectively) lie either side of the wall temperature once a steady, periodic state is achieved. Simulations were continued until temperatures at TDC were within 0.1 K for successive cycles. Calculations were conducted for both geometries with both air and helium as working fluids.

Similar conditions were applied for gas springs with an internal grid, but an adiabatic ('zeroGradient') condition was applied to the grid itself so as not to create additional heat transfer area.

3.3.2 Calculations with valves

For the simulations with valves, the inlet air condition was set to 300 K and 1 bar. The delivery pressure (at which the outlet valve was opened) was set at either 6 or 7 bar. The working fluid was air and geometry 2 was used for all valve cases. The temperature of the wall once a real system reaches a steady state is not known in advance and depends on many factors (e.g., piston speed, level of insulation etc.). In this steady state it is expected that the wall temperature will lie between the inlet temperature (fixed at 300 K) and delivery temperature, the latter depending on pressure ratio and rotational speed. To aid comparison with gas springs, the delivery temperature is first estimated using the polytropic index n determined from the gas spring results using,

$$n = \frac{\ln(p_{\max} / p_{\min})}{\ln(V_{\max} / V_{\min})} \qquad (2)$$

The dependence of n on piston (rotational) speed is shown in Fig. 5 where the compression and expansion processes are seen to move from isothermal towards adiabatic as the speed is increased, as expected. The estimated delivery temperature is given by,

$$T_{2*} = T_1 \left(\frac{p_2}{p_1} \right)^{(n-1)/n} \qquad (3)$$

where 1 and 2 denote inlet and delivery respectively. The wall temperature is then set and fixed at $T_{\text{wall}} = (T_1 + T_{2*}) / 2$. The resulting temperatures for the cylinder walls are given in Table 2.

Outlet pressure (bar)	Piston speed (rpm)	Wall temperature (K)
7	1500	410
7	60	401
6	1500	398

Table 2: Specified wall temperatures for valve simulations

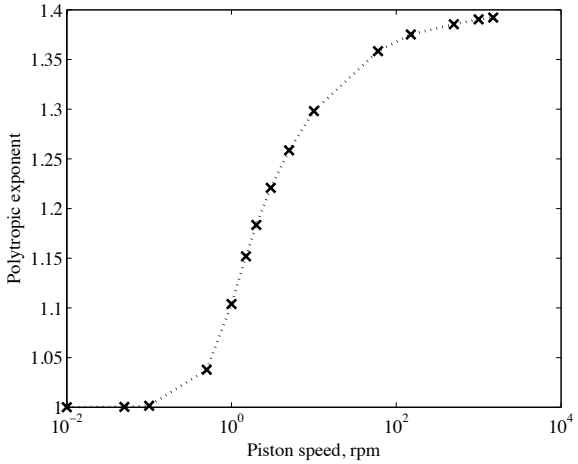

Figure 5: Polytropic exponent against piston speed

Simulations reached a steady state after several cycles with the lowest temperature close to the inlet value. Calculations were stopped when the change in temperature at TDC from one cycle to the next was smaller than 0.5 K.

4 Non dimensional speed and loss

To aid comparison between different geometries, results are expressed in dimensionless terms where appropriate. The Peclet number provides a suitable non-dimensional speed for heat transfer problems and is given by,

$$\mathrm{Pe}_{\omega} = \omega D_h^2 / 4\alpha \qquad (4)$$

where D_h is the hydraulic diameter, $\alpha = (\alpha_{\max} + \alpha_{\min}) / 2$ is the average thermal diffusivity and ω is the rotational speed (in rad s^{-1}). D_h is computed from

$$D_h = 4V_0 / A_{w,0} \qquad (5)$$

where V_0 and $A_{w,0}$ are the gas volume and wall surface area respectively at mid stroke.

For describing the thermodynamic loss due to irreversibility in a gas spring, an efficiency decrement Ψ is used, defined by

$$\Psi = \frac{\oint p\,dV}{\oint |p\,dV|} \qquad (6)$$

This is equivalent to the lost work per cycle normalised by the sum of the compression and expansion work and therefore reflects the average loss in efficiency for a compression or expansion process [6].

5 Simulation results and discussion

5.1 Gas spring results

Figure 6 shows the efficiency decrement calculated according to eq. (6) for a gas spring (geometry 1) with and without a grid. It can be seen that the grid increases the loss at high Peclet number whereas it has little effect at low speed. Part of the additional loss is due to enhanced heat transfer and part is due to viscous dissipation. The latter component can be estimated by undertaking calculations with adiabatic wall conditions, for which there can be no losses due to heat transfer. As shown in the figure, whilst the resulting loss for a simple gas spring remains close to zero, that with a grid rises sharply at high speeds, as would be expected from straightforward stagnation pressure loss considerations. Figure 6 also shows the difference between results obtained with isothermal and adiabatic cylinder walls for the case with a grid. This shows what fraction of the additional loss stems from heat transfer. The increase observed at high speed (roughly a factor of two at the highest Peclet number) is significant since compressors and expanders for PTES applications would most likely be designed to operate in this regime. Furthermore, as described in more detail in Ref. [8], the gas velocity at the grid is necessarily quite low (because the grid must be within the dead space, and because velocities fall roughly linearly to zero at the cylinder head) and so the impact of the grid on heat transfer is likely to be less than that for flow through the valves of a real compressor.

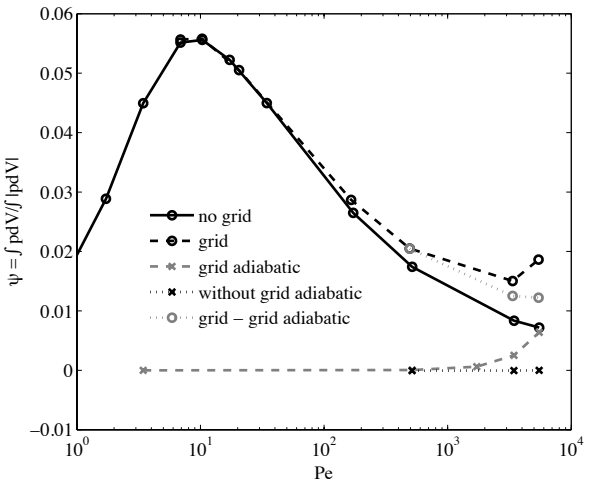

Figure 6: Efficiency decrement Ψ (eq. 6) against Peclet number for a gas spring with and without a turbulence-inducing grid [8].

5.2 Simulations with valves

5.2.1 Pressure and mass variations

Figure 7 shows the computed *p-V* diagrams for a compressor operating with valves. Results are shown for outlet pressures of 6 and 7 bar at 1500 rpm and for 7 bar at 60 rpm. According to the gas spring results, these speeds are near to the adiabatic regime (as indicated in Fig. 5), which is the region of interest for PTES devices. (Note that the volume in the figure is for the entire cylinder, not just for the simulated quarter.) The air inside the cylinder is compressed between points 1 and 2 and when the internal pressure reaches the set delivery pressure the valve in the piston face is opened. The pressure remains roughly constant whilst the valve is open: fluctuations do occur immediately after opening, but these are small (e.g., the maximum amplitude for the 7 bar case at 1500 rpm was 50 mbar). When the piston reaches TDC the delivery valve closes (point 3) and the expansion starts. The inlet valve on the cylinder head opens once the pressure has fallen to 1 bar (point 4) and air is then drawn into the cylinder until the valve closes at BDC. The difference in the *p-V* diagrams for the 7 bar cases at different piston speeds is small: valves open very slightly later for the lower speed case. Very low speed cases have not yet been simulated (since they are not of practical interest in the current context), but it is likely that they would show more substantive delays in valve timing because the compression and expansion strokes would then approach isothermal processes, as indicated by Fig. 1.

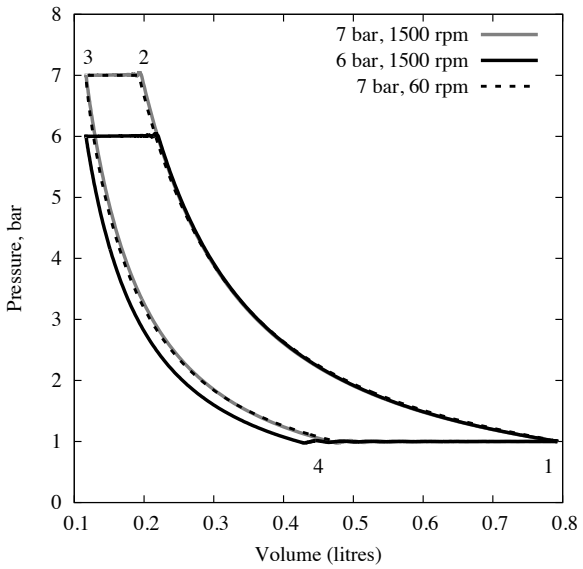

Figure 7: *p-V* diagrams for 6 and 7 bar outlet pressure

Figure 8 shows a comparison of pressure variations against crank angle for simulations with valves and with a simple gas spring. To aid comparison (and to account for the different boundary conditions described in sections 3.3.1 and 3.3.2), pressures have been normalised by the value at BDC in each case. For the compression process, the variation in pressure ratio is similar in all cases up to the point at which the outlet

opens, reflecting near-isentropic ($pV^{\gamma} \approx \text{const.}$) processes for this part of the cycle.

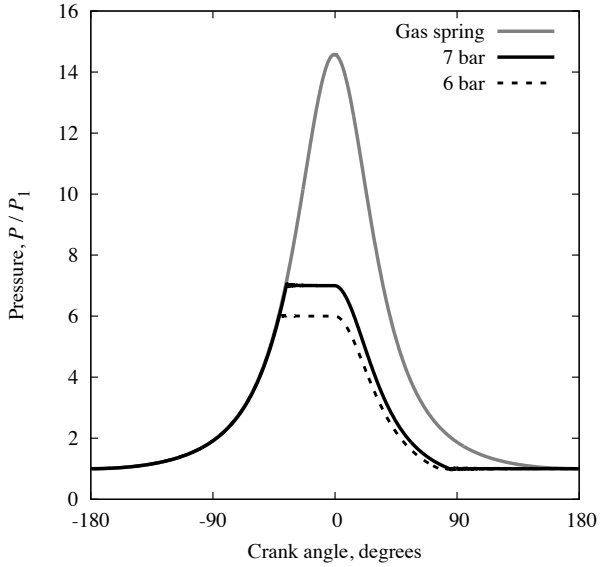

Figure 8: Pressure vs. crank angle at 1500 rpm for outlet pressures of 7 bar and 6 bar and for a gas spring.

For the expansion processes – i.e., from TDC (0°) onwards – differences are mainly due to the different initial pressures and the different masses of gas within the cylinder. Figure 9 shows how this mass varies throughout the cycle: it is constant during the compression and expansion processes (as expected, the valves being closed), but obviously increases during intake (4 – 1) and decreases during delivery (2 – 3). The mass transported per cycle (i.e., the difference between the maximum and minimum values) decreases with delivery pressure, due mainly to the reduced length of the delivery and intake strokes at higher delivery pressure, as shown in Fig. 7. However, it is also clear from Fig. 9 that the mass transported per cycle depends on the rotational speed. For the two cases at 7 bar, the mass inflow during intake is significantly less at 60 rpm than at 1500 rpm, suggesting that volumetric efficiency *increases* with rotational speed. Valve pressure losses are small with the current set up, so the volumetric efficiency is affected chiefly by heat transfer from the warm cylinder walls to the cooler charge air. This is greater at lower speeds, leading to hotter, less dense charge air in the 60 rpm case. The increased temperature at point 1 for this case has a knock-on effect around the cycle and has implications for the mixing loss (occurring between states 4 and 1) as well as heat transfer rates. The extent of these effects will however depend on the assumed wall temperature and so further calculations are required to obtain a full picture.

The mass flow rate through the compressor is given by the product of the crank speed (in revolutions per second) and the mass transported per cycle. Evidently, changing the crank speed enables independent control of the mass flow rate and

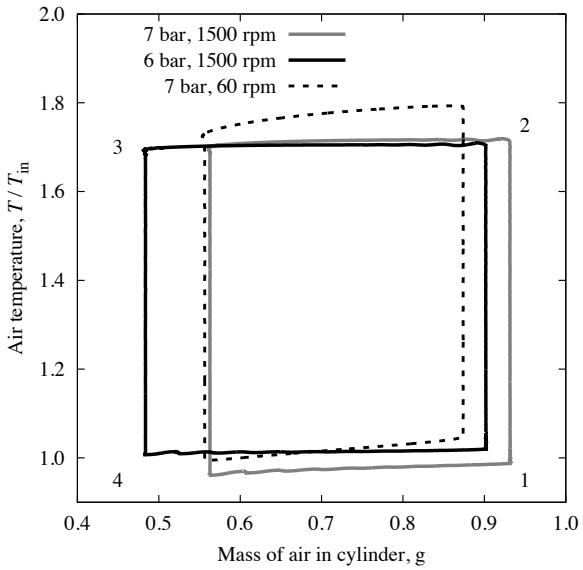

Figure 9: Temperature vs. mass of air in the cylinder

pressure ratio, but there may be scenarios for which this is not practically possible – for example when the compressor is driven by a synchronous motor. In passing it is worth noting that some additional control of mass flow may be achieved by delaying closure of the intake valve until after BDC, though this possibility has not yet been simulated.

5.2.2 Heat fluxes and temperature profiles

Figure 10 shows the gas-wall temperature difference for the three valve flow cases. (Note that the gas temperature is the mass-averaged value within the cylinder.) Gas spring results for the same rotational speeds are also shown. All cases have similar overall temperature variations, but there are nonetheless significant differences in the detail. For example, for the two curves at 7 bar, the lower speed case results in higher gas temperatures throughout the cycle due to the greater heat transfer to the inlet air, as described above. Likewise, for the 1500 rpm cases, the temperature is roughly constant when the valves are open, whilst for the gas spring it continues to change due to continued compression or expansion. These differences will clearly affect heat transfer rates such that direct comparison of heat fluxes would be misleading. The main interest is whether the *mechanisms* of heat transfer are affected by the valve flows, and so in an attempt to separate out the effects of the changed temperature variations over the cycle, heat transfer coefficients for the (curved surface) liner have been computed. These are defined by

$$h = \frac{\dot{Q}_l}{A_l (T_w - T_b)} \qquad (7)$$

where A_l is the instantaneous liner area in contact with the gas and T_b is the bulk (mass-averaged) air temperature.

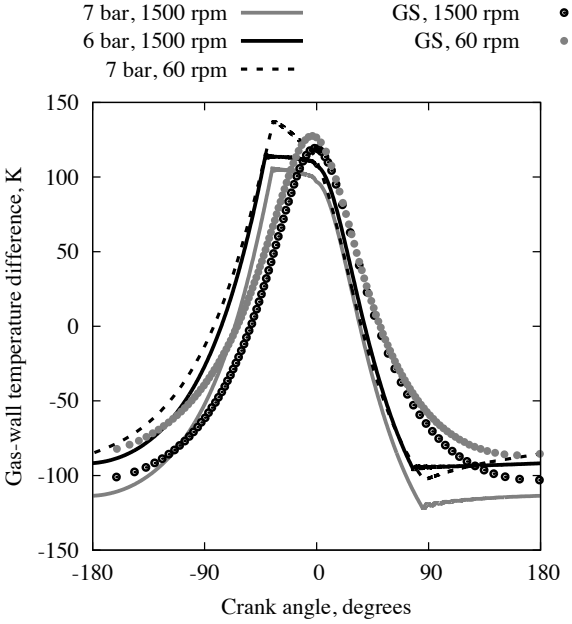

Figure 10: Difference between the mass-averaged gas and wall temperature vs. crank angle (GS: gas spring).

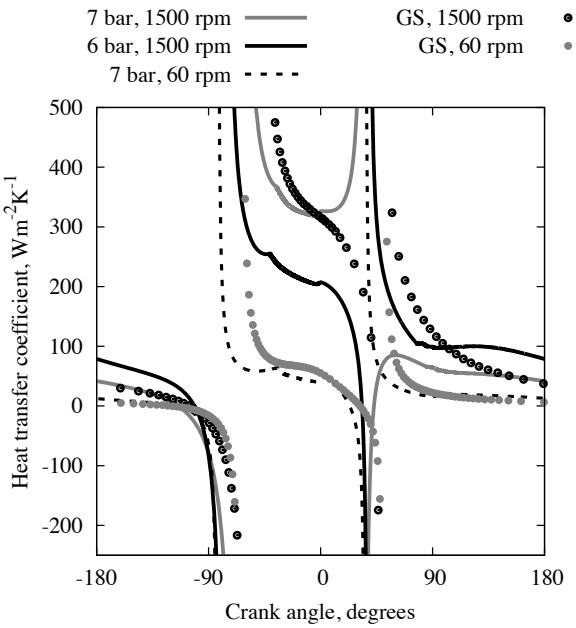

Figure 11: The cylinder liner heat transfer coefficient (eq. 7) vs. crank angle (GS: gas spring).

Figure 11 shows variations in the heat transfer coefficient h for the various cases. It is notable that h becomes infinite at certain stages and is also negative over parts of the cycle. This is a well-known phenomenon for unsteady heat transfer, especially in the context of gas springs (see for example Ref. [16]) and stems from the gas temperature gradient near the wall being out of phase with the (bulk) gas-wall temperature difference. This in turn is a consequence of the interaction between work and heat transfers to and from the gas, as discussed further in [16].

It is clear from Fig. 11 that there are significant differences between the cases. Broadly, higher delivery pressure results in variations of h that are closer to those of a gas spring, as would be expected, but further calculations are required to confirm this trend. Significant qualitative differences are evident between the valve and gas spring cases: for example, for the 7 bar case at 1500 rpm, h tends to $+\infty$ (heat transfer in phase with ΔT) in the initial stages of expansion just after TDC, whereas it reduces and then becomes negative (tending to $-\infty$) for the gas spring. Such differences necessarily stem from the effect that the valve events have on the local temperature profiles, examples of which are shown in Fig. 12 for the piston at BDC. This point of the cycle is at the end of the expansion for the gas spring and at the end of the intake stroke for the compressor. Mean gas temperatures are thus near their lowest values, but note that results are shown close to the cylinder head and to the piston face where the gas is warmer than in the core of the cylinder. The unusual, wavy profile for the valved case near to the cylinder head (i.e., where the inlet valve is situated) is due to the jets of inlet air entering through the rectangular apertures. (Note that the inlet gas temperature is roughly 100 K below T_{wall}).

It is not surprising that these jets and the ensuing mixing have a significant impact on radial temperature profiles and thus on heat transfer. However, whereas such mixing might normally be expected to enhance heat transfer rates, this is not always the case in the current context. For example, if the wall temperature gradient is in the opposite direction to the bulk temperature difference then mixing may result in reduced heat exchange. Accordingly, bulk-temperature-based heat transfer coefficients are sometimes higher and sometimes lower for the compressor than for the gas spring, as seen in Fig. 11.

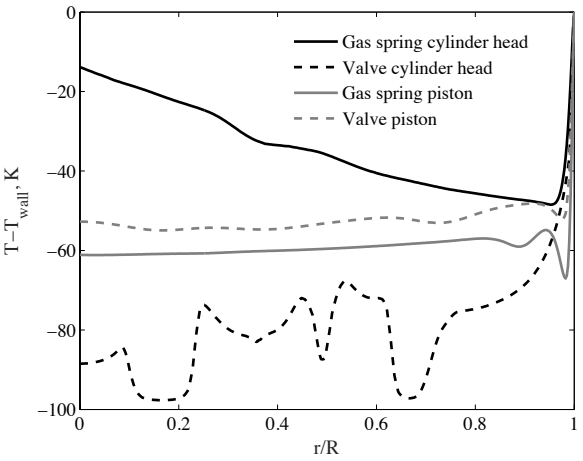

Figure 12: Radial profiles of gas temperature (relative to T_{wall}) 0.5mm from the piston and the cylinder head at BDC. Results are for 1500 rpm (and 7 bar, valve).

6 Conclusions

CFD simulations using the OpenFoam software have been undertaken in order to compare and better understand the heat transfer processes occurring in (a) simple gas springs, (b) a gas spring with an internal grid inserted within the dead space and (c) a reciprocating compressor with functioning valves. In line with experimental findings from other sources, the simple gas spring results show processes that are almost reversible for very low and very high piston speeds, corresponding to the isothermal and adiabatic limits respectively, whereas a hysteresis loss is predicted at intermediate speeds. The latter may be a significant fraction of the compression work done per cycle, and is due almost entirely to irreversible heat transfer between the gas and the cylinder walls. This was shown by undertaking calculations with adiabatic walls, for which predicted losses were very small.

The inclusion of a grid was intended to provide a preliminary indication of the effects of valve flows by generating eddying motions and additional turbulence within the cylinder. The results showed an increase in the hysteresis loss at high speed due to a combination of stagnation pressure drop through the grid and enhanced heat transfer with the walls. These two effects were separated by again undertaking adiabatic wall calculations, which showed that the heat transfer effect was responsible for a modest increase in hysteresis loss for the near-adiabatic regime of interest.

Simulations with a novel, uni-flow valve arrangement (based on a design intended for PTES applications) were undertaken at three operating conditions. These showed that the mass transported per cycle and the instantaneous heat transfer coefficients were significantly affected by both the delivery pressure and the piston speed. Direct comparisons with simple gas springs are difficult to interpret but suggest that the valve flows enhance heat transfer coefficients over some parts of the cycle, but reduce them at others. This would seem to stem from the impact of mixing on the complicated profiles of temperature near the wall, which for flows with both heat and work transfer may exhibit gradients that oppose the bulk gas-wall temperature difference. These preliminary results for valved devices also point the way to future simulations aimed at establishing exergetic losses and, in particular, (and in contrast to gas spring simulations) highlight the need to consider the wall temperature as an additional parameter.

Acknowledgements

This work was supported by the UK Engineering and Physical Sciences Research Council (reference number. EP/J006246/1). It was carried out using the University of Cambridge's Darwin Supercomputer provided by Dell Inc. using Strategic Research Infrastructure Funding from the Higher Education Funding Council for England and funding from the Science and Technology Facilities Council.

References

[1] R. W. Moss, A. P. Roskilly, and S. K. Nanda, "Reciprocating Joule-cycle engine for domestic CHP systems," *Appl. Energy*, vol. 80, no. 2, pp. 169–185, Feb. 2005.

[2] A. J. White, "Thermodynamic analysis of the reverse Joule-Brayton cycle heat pump for domestic heating," *Appl. Energy*, vol. 86, pp. 2443–2450, 2009.

[3] B. Kongtragool and S. Wongwises, "A review of solar-powered Stirling engines and low temperature differential Stirling engines," *Renew. Sustain. Energy Rev.*, vol. 7, no. 2, pp. 131–154, Apr. 2003.

[4] A. White, G. Parks, and C. N. Markides, "Thermodynamic analysis of pumped thermal electricity storage," *Appl. Therm. Eng.*, vol. 53, no. 2, pp. 291–298, May 2013.

[5] U. Lekic and J. B. W. Kok, "Heat Transfer and Fluid Flows in Gas Springs," *Open Thermodyn. J.*, vol. 4, pp. 13–26, 2010.

[6] R. Mathie, C. N. Markides, and A. J. White, "A Framework for the Analysis of Thermal Losses in Reciprocating Compressors and Expanders," *Heat Transf. Eng.*, vol. 35, no. 16–17, pp. 1435–1449, 2014.

[7] A. A. Kornhauser and J. L. Smith, "Application of a Complex Nusselt Number to Heat Transfer During Compression and Expansion," *Journal of Heat Transfer*, vol. 116. p. 536, 1994.

[8] C. Willich, C. N. Markides, and A. J. White, "An investigation of heat transfer losses in reciprocating devices," *Appl. Therm. Eng.*, 2016.

[9] H. G. Weller, G. Tabor, H. Jasak, and C. Fureby, "A tensorial approach to computational continuum mechanics using object-oriented techniques," *Comput. Phys.*, vol. 12, no. 6, p. 620, 1998.

[10] J. E. Bardina, P. G. Huang, and T. J. Coakley, "Turbulence Modeling Validation, Testing, and Development," 1997.

[11] I. Pantokratoras and C. Arapatsakos, "Turbulence Models Comparison for the Numerical Study of the Air Flow, an Internal Combustion Engine," in *Advances in Engineering Mechanics and Material*, pp. 178– 184, 2014.

[12] B. Andersson, R. Andersson, L. Hakansson, M. Mortensen, R. Sudiyo, and B. Van Wachem, *Computational Fluid Dynamics for Engineers*. 2011.

[13] H. J. Aguerre, S. Marquez Damian, J. M. Gimenez, and N. M. Nigro, "Modeling of Compressible Fluid Problems with OpenFOAM using Dynamic Mesh Technology," *Mecánica Comput.*, vol. XXXII, pp. 995–1011, 2013.

[14] A. A. Kornhauser and J. L. Smith, "The Effects of Heat Transfer on Gas Spring Performance," *J. Energy Resour. Technol.*, vol. 115, no. 1, pp. 70–75, Mar. 1993.

[15] J. Howes, "Concept and Development of a Pumped Heat Electricity Storage Device," *Proc. IEEE*, vol. 100, no. 2, pp. 493–503, Feb. 2012.

[16] B. Lawton, 'Effect of Compression and Expansion on Instantaneous Heat Transfer in Reciprocating Internal Combustion Engines', *Proc. Inst. Mech. Eng. Part J. Power Energy*, vol. 201, no. 3, pp. 175–186, 1987.